Characteristics of total gaseous mercury (TGM) concentrations in an industrial complex in southern Korea: Impacts from local sources

Yong-Seok Seo[1,2], Seung-Pyo Jeong[1], Thomas M. Holsen[3], Young-Ji Han[4], Eunhwa Choi[5], Eun Ha Park[1], Tae Young Kim[1], Hee-Sang Eum[1], Dae Gun Park[1], Eunhye Kim[6], Soontae Kim[6], Jeong-Hun Kim[7], Jaewon Choi[8], Seung-Muk Yi[1,2,*]

[1]Department of Environmental Health, Graduate School of Public Health, Seoul National University, 1 Gwanak, Gwanak-ro, Gwanak-gu, Seoul 151-742, South Korea

[2]Institute of Health and Environment, Seoul National University, 1 Gwanak, Gwanak-ro, Gwanak-gu, Seoul 151-742, South Korea

[3]Department of Civil and Environmental Engineering, Clarkson University, Potsdam, NY13699, USA

[4]Department of Environmental Science, Kangwon National University, 192-1, Hyoja-2-dong, Chuncheon, Kangwondo, 200-701, South Korea

[5]Asian Institute for Energy, Environment & Sustainability, Seoul National University, 1 Gwanak-ro, Gwanak-gu, Seoul 151-742, South Korea

[6]Department of Environmental, Civil and Transportation Engineering, Ajou University, Woncheon-dong, Yeongtong-gu, Suwon, 443-749, South Korea

[7]Division of Air Pollution Engineering, Department of Climate and Air Quality Research, National Institute of Environmental Research, Hwangyong-ro 42, Seogu, Incheon, 404-708, South Korea

[8]University of Pennsylvania, Philadelphia, PA19104, USA

[*]Address correspondence to Dr. Seung-Muk Yi, Graduate School of Public Health, Seoul National University, 1 Gwanak, Gwanak-ro, Gwanak-gu, Seoul 151-742, South Korea
E-mail) yiseung@snu.ac.kr
Telephone) 82-2-880-2736
Fax) 82-2-745-9104

45   **Abstract**

46   Total gaseous mercury (TGM) concentrations were measured every 5 min in Pohang,

47   Gyeongsangbuk-do, Korea during summer (17 August~23 August 2012), fall (9 October~17

48   October 2012), winter (22 January ~29 January 2013), and spring (26 March~3 April 2013)

49   to: 1) characterize the hourly and seasonal variations of atmospheric TGM concentrations, 2)

50   identify the relationships between TGM and co-pollutants, and 3) identify likely source

51   directions and locations of TGM using conditional probability function (CPF), conditional

52   bivariate probability function (CBPF) and total potential source contribution function

53   (TPSCF).

54   The TGM concentration was statistically significantly highest in fall (6.7 ± 6.4 ng m^{-3}),

55   followed by spring (4.8 ± 4.0 ng m^{-3}), winter (4.5 ± 3.2 ng m^{-3}) and summer (3.8 ± 3.9 ng m^{-3}

56   ^{3}). There was a weak but statistically significant negative correlation between the TGM

57   concentration and ambient air temperature *(r = -0.08) (p < 0.05).* Although the daytime

58   temperature (14.7 ± 10.0 ℃) was statistically significantly higher than that in the nighttime

59   (13.0 ± 9.8 ℃) ($p < 0.05$), the daytime TGM concentration (5.3 ± 4.7 ng m^{-3}) was statistically

60   significantly higher than those in the nighttime (4.7 ± 4.7 ng m^{-3}) ($p < 0.01$), possibly due to

61   local emissions related to industrial activities and activation of local surface emission

62   sources. The observed ΔTGM/ΔCO was significantly lower than that of Asian long-range

63   transport, but similar to that of local sources in Korea and in US industrial events suggesting

64   that local sources are more important than that of long-range transport. CPF, CBPF and

65   TPSCF indicated that the main sources of TGM were iron and manufacturing facilities, the

66   hazardous waste incinerators and the coastal areas.

70 **1. Introduction**

71   Mercury (Hg) is an environmental toxic and bioaccumulative trace metal whose emissions

72 to the environment have considerably increased due to anthropogenic activities such as

73 mining and combustion processes (Pirrone et al., 2013; Streets et al., 2011). Hg can be

74 globally distributed from the sources through atmospheric transport as gaseous elemental

75 form (Bullock et al., 1998; Mason and Sheu, 2002). However, the origins of atmospheric

76 mercury are local and regional (Choi et al., 2009) as well as hemispherical and global

77 (Durnford et al., 2010). In addition to the general background concentration of Hg in the

78 global atmosphere, local Hg emissions contribute to the Hg burden and it contribute to the

79 background concentration much of which represents anthropogenic releases accumulated

80 over the decades (UNEP, 2002).

81   Hg in the atmosphere exists in three major inorganic forms including gaseous elemental

82 mercury (GEM, Hg^0), gaseous oxidized mercury (GOM, Hg^{2+}) and particulate bound

83 mercury (PBM, Hg(p)). GEM which is the dominant form of Hg in ambient air, (>95%) has a

84 relatively long residence time (0.5~2 years) due to its low reactivity and solubility (Schroeder

85 and Munthe, 1998). However, GOM has high water solubility and relatively strong surface

86 adhesion properties (Han et al., 2005), so it has a short atmospheric residence time (~days).

87 PBM is associated with airborne particles such as dust, soot, sea-salt aerosols, and ice crystals

88 (Lu and Schroeder, 2004) and is likely produced, in part, by adsorption of GOM species such

89 as $HgCl_2$ onto atmospheric particles (Gauchard et al., 2005; Lu and Schroeder, 2004; Sakata

90 and Marumoto, 2005; Seo et al., 2012; Seo et al., 2015).

91   Atmospheric Hg released from natural (e.g., volcanoes, volatilization from aquatic and

92 terrestrial environments) (Pirrone et al., 2010; Strode et al., 2007) and anthropogenic sources

93 (e.g., coal combustion, cement production, ferrous and non-ferrous metals manufacturing

4

94   facilities, waste incineration and industrial boilers) (Pacyna et al., 2010; Pacyna et al., 2006;

95   Pacyna et al., 2003; Pirrone et al., 2010; Zhang et al., 2015) when introduced into terrestrial

96   and aquatic ecosystem through wet and dry deposition (Mason and Sheu, 2002) can undergo

97   various physical and chemical transformations before being deposited. Its lifetime in the

98   atmosphere depends on its reactivity and solubility so that, depending on its form, it can have

99   impacts on local, regional and global scales (Lin and Pehkonen, 1999; Lindberg et al., 2007).

100 A portion of the Hg deposited in terrestrial environments through direct industrial discharge

101 or atmospheric deposition is transported to aquatic system through groundwater and surface

102 water runoff (Miller et al., 2013). A previous study also reported that Hg directly released

103 into terrestrial and aquatic ecosystems from industrial effluent has influenced surface water,

104 sediment and biological tissue (Flanders et al., 2010). Significant spatial variations in

105 atmospheric Hg deposition near urban and industrial areas are due to local anthropogenic

106 sources including municipal waste incinerators, medical waste incinerators, electric power

107 generating facilities and cement kilns (Dvonch et al., 1998), ferrous and non-ferrous metal

108 processing, iron and steel manufacturing facilities, oil and coal combustion (Hoyer et al.,

109 1995), and other forms of industrial combustion (Brown et al., 2015). Miller et al. (2013) also

110 reported that local sources of elemental Hg are typically industrial processes including retort

111 facilities used in the mercury mining industry to convert Hg containing minerals to elemental

112 Hg and chlor-alkali facilities.

113   The annual average national anthropogenic Hg emissions from South Korea in 2007 have

114 been estimated to be 12.8 tons (range 6.5 to 20.2 tons); the major emission sources are coal

115 combustion in thermal power plants (25.8%), oil refineries (25.5%), cement kilns (21%),

116 incinerators (19.3%) including sludge incinerators (4.7%), municipal waste incinerators

117 (MWIs) (3%), industrial waste incinerators (IWIs) (2.7%), hospital/medical/infectious waste

5

118 incinerators (HMIWIs) (8.8%), and iron manufacturing (7%) (Kim et al., 2010). Global

119 anthropogenic Hg emissions were estimated to be 1960 tons in 2010 with East and Southeast

120 Asia responsible for 777 tons (39.7%) (19.6 tons for Japan and 8.0 tons for South Korea)

121 (AMAP/UNEP, 2013). China is the largest Hg emitting country in the world, contributing

122 more than 800 tons (~ 40%) of the total anthropogenic Hg emissions (UNEP, 2008).

123 Background atmospheric Hg concentrations in the northern hemisphere have decreased

124 since 1996 (Slemr et al., 2003), as measured at the Global Atmosphere Watch (GAW) station

125 at Mace Head, Ireland (Ebinghaus et al., 2011) and at the Canadian Atmospheric Mercury

126 Network (CAMNet) (Temme et al., 2007). In urban areas in South Korea atmospheric TGM

127 concentrations have also decreased over the last few decades due to the reduced fossil fuel

128 (mainly anthracite coal) consumption (Kim et al., 2016; Kim and Kim, 2000). However, this

129 decreasing trend is inconsistent with steady or increasing global anthropogenic Hg emissions

130 since 1990 in the northern hemisphere (Streets et al., 2011; Weigelt et al., 2015; Wilson et al.,

131 2010). A previous study reported that the global anthropogenic Hg emissions are increasing

132 with an average of 1.3% annual growth without including the artisanal and small-scale

133 production sector (Muntean et al., 2014).

134 Receptor models are often used to identify sources of air pollutants and are focused on the

135 pollutants behavior in the ambient environment at the point of impact (Hopke, 2003). In

136 previous studies, conditional probability function (CPF), which utilizes the local wind

137 direction, and potential source contribution function (PSCF), which utilizes longer backward

138 trajectories (typically 3-5 days), combined with concentration data were used to identify

139 possible transport pathways and source locations (Hopke, 2003). While PSCF has been used

140 primarily to identify regional sources, it has also been used to identify local sources (Hsu et

141 al., 2003).

6

142   The objectives of this study were to characterize the hourly and seasonal variations of

143   atmospheric TGM (the sum of the GEM and the GOM) concentrations, to identify the

144   relationships between TGM and co-pollutant concentrations, and to identify likely source

145   directions and locations of TGM using CPF, conditional bivariate probability function

146   (CBPF) and total PSCF (TPSCF).

147

148   **2. Materials and methods**

149   *2.1. Sampling and analysis*

150   TGM concentrations were measured on the roof of the Korean Federation of

151   Community Credit Cooperatives (KFCCC) building (latitude: 35.992°, longitude: 129.404°,

152   ~10 m above ground) in Pohang city, in Gyeongsangbuk-do, a province in eastern South

153   Korea. Gyeongsangbuk-do has a population of 2.7 million (5% of the total population and the

154   third most populated province in South Korea) and an area of 19,030 km^2 (19% of the total

155   area of South Korea and the largest province geographically in South Korea). Pohang city has

156   a population of 500,000 (1% of the total population in South Korea) and an area of 605.4 km^2

157   (1.1% of the total area in South Korea). It is heavily industrialized with the third largest steel

158   manufacturing facility in Asia and the fifth largest in the world. There are several iron and

159   steel manufacturing facilities including electric and sintering furnaces using coking in

160   Gyeongsangbuk-do including Pohang. In addition, there are several coke plants around the

161   sampling site. The Hyungsan River divides the city into a residential area and the steel

162   complex. Hg emissions data from iron and steel manufacturing, and a hazardous waste

163   incinerator were estimated based on a previous study (Kim et al., 2010) (Fig. 1).

164   TGM concentrations were measured every 5 min during summer (17 August~23 August

165   2012), fall (9 October~17 October 2012), winter (22 January ~29 January 2013), and spring

166   (26 March~3 April 2013) using a mercury vapor analyzer (Tekran 2537B) which has two

167   gold cartridges that alternately collect and thermally desorb mercury. Ambient air at a flow

168   rate of 1.5 L min^{-1} was transported through a 3 m-long heated sampling line (1/4" OD Teflon)

169   in to the analyzer. The sampling line was heated at about 50 ℃ using heat tape to prevent

170   water condensation in the gold traps because moisture on gold surfaces interferes with the

171   amalgamation of Hg (Keeler and Barres, 1999). Particulate matter was removed from the

172   sampling line by a 47 mm Teflon filter.

173

174   *2.2. Meteorological data*

175   Hourly meteorological data (air temperature, relative humidity, and wind speed and

176   direction) were obtained from the Automatic Weather Station (AWS) operated by the Korea

177   Meteorological Administration (KMA) (http://www.kma.go.kr) (6 km from the site). Hourly

178   concentrations of NO_2, O_3, CO, PM_{10} and SO_2 were obtained from the National Air Quality

179   Monitoring Network (NAQMN) (3 km from the site) (Fig. 1).

180   Meteorological Setting. Fig. S1 shows the frequency of counts of measured wind direction

181   occurrence by season during the sampling period. The predominant wind direction at the

182   sampling site was W (20.9%) and WS (19.2%), and calm conditions of wind speed less than

183   1 m s^{-1} occurred 7.6% of the time. Compared to other seasons, however, the prevailing winds

184   in summer were N (17.0%), NE (16.4%), S (16.4%), and SW (15.8%).

185

186   *2.3. QA/QC*

187   Automated daily calibrations were carried out for the Tekran 2537B using an internal

188   permeation source. Two-point calibrations (zero and span) were separately performed for

189   each gold cartridge. Manual injections were performed prior to every field sampling

8

190 campaign to evaluate these automated calibrations using a saturated mercury vapor standard.

191 The relative percent difference (RPD) between automated calibrations and manual injections

192 was less than 2%. The recovery measured by directly injecting known amounts of four

193 mercury vapor standards when the sample line was connected to zero air ranged from 92 to

194 110% (99.4 ± 5.2% in average).

195

196 **3. Model descriptions**

197 *3.1. Conditional Probability Function (CPF)*

198 CPF was originally performed to determine which wind directions dominate during high

199 concentration events to evaluate local source impacts (Ashbaugh et al., 1985). It has been

200 successfully used in many previous studies (Begum et al., 2004; Kim et al., 2003a; Kim et al.,

201 2003b; Xie and Berkowitz, 2006; Zhao et al., 2004; Zhou et al., 2004). CPF estimates the

202 probability that the measured concentration will exceed the threshold criterion for a given

203 wind direction. The CPF is defined as follows Eq. (1).

204
205 $$CPF_{\Delta\theta} = \frac{m_{\Delta\theta|C \geq x}}{n_{\Delta\theta}} \qquad\qquad (1)$$

206

207 where, $m_{\Delta\theta}$ is the number of samples from the wind sector θ having concentration C greater

208 than or equal to a threshold value x, and $n_{\Delta\theta}$ is the total number of samples from wind sector

209 $\Delta\theta$. In this study, 16 sectors ($\Delta\theta = 22.5°$) were used and calm winds (≤ 1 m s^{-1}) were excluded

210 from the analysis. The threshold criterion was set at above the overall average TGM

211 concentration (5.0 ng m^{-3}). Thus, CPF indicates the potential for winds from a specific

212 direction to contribute to high air pollution concentrations.

9

213

214 *3.2. Conditional Bivariate Probability Function (CBPF)*

215 CBPF couples ordinary CPF with wind speed as a third variable, allocating the measured

216 concentration of pollutant to cells defined by ranges of wind direction and wind speed rather

217 than to only wind direction sectors.

218 The CBPF is defined as follows Eq. (2).

219

220 $$CBPF_{\Delta\theta,\Delta u} = \frac{m_{\Delta\theta,\Delta u}|_{C \geq x}}{n_{\Delta\theta,\Delta u}} \tag{2}$$

221

222 where, $m_{\Delta\theta,\Delta u}$ is the number of samples in the wind sector $\Delta\theta$ with wind speed interval Δu

223 having concentration C greater than a threshold value x, and $n_{\Delta\theta\Delta u}$ is the total number of

224 samples in that wind direction-speed interval. The threshold criterion was set at above the

225 overall average TGM concentration (5.0 ng m^{-3}). The extension to the bivariate case can

226 provide more information on the nature of the sources because different source types such as

227 stack emission sources and ground-level sources can have different wind speed dependencies

228 (prominent at high and low wind speed, respectively). More detailed information is described

229 in a previous study (Uria-Tellaetxe and Carslaw, 2014).

230

231 *3.3. Potential Source Contribution Function (PSCF)*

232 The PSCF model has been extensively and successfully used in the previous studies to

233 identify the likely source areas (Cheng et al., 1993; Han et al., 2004; Hopke et al., 2005; Lai

234 et al., 2007; Lim et al., 2001; Poissant, 1999; Zeng and Hopke, 1989). The PSCF is a simple

235 method that links residence time in upwind areas with high concentrations through a

236 conditional probability field and was originally developed by Ashbaugh et al. (1985). PSCF$_{ij}$

10

237   is the conditional probability that an air parcel that passed through the ijth cell had a high

238   concentration upon arrival at the monitoring site and is defined as the following Eq. (3).

239

240                                     $$PSCF_{ij} = \frac{m_{ij}}{n_{ij}}$$ (3)

241

242   where, n_{ij} is the number of trajectory segment endpoints that fall into the ij-th cell, and m_{ij} is the

243   number of segment endpoints in the same grid cell (ij-th cell) when the concentrations are higher

244   than a criterion value as measured at the sampling site.

245   High PSCF values in those grid cells are regarded as possible source locations. Cells including

246   emission sources can be identified with conditional probabilities close to one if trajectories that

247   have crossed the cells efficiently transport the released pollutant to the receptor site. Therefore,

248   the PSCF model provides a tool to map the source potentials of geographical areas.

249   The criterion value of PSCF for TGM concentration was set at above the overall average

250   concentration (5.0 ng m^{-3}) to identify the emission sources associated with high TGM

251   concentrations and provide a better estimation and resolution of source locations during the

252   sampling periods. The geographic area covered by the computed trajectories was divided into

253   an array of 0.05° latitude by 0.05° longitude grid cells. As will be discussed in Section 5.3, 24

254   h backward trajectories starting at every hour at a height of 10, 50, and 100 m above ground

255   level were computed using the vertical velocity model because local sources are more

256   important than that of long-range transport in this study (It should be noted that PSCF results

257   using 48 h backward trajectories had similar results as the 24 h backward trajectories). Each

258   trajectory was terminated if they exit the model top (5,000m), but advection continues along

259   the surface if trajectories intersect the ground. To generate horizontally highly resolved

260   meteorological inputs for trajectory calculations, the Weather Research and Forecast (WRF)

261   model was used to generate a coarse domain at a resolution of 27 km and a nested domain at

262   a horizontal resolution of 9 km, which geographically covers northeast Asia and the southern

263   part of the Korean Peninsula, respectively. The nested domain has 174 columns in the east-

264   west direction and 114 rows in the north-south direction. PSCF was calculated with 9 km

265   meteorological data.

266   In this study, TPSCF which incorporates probability from above different starting

267   heights was calculated since backward trajectories starting at different heights traverse

268   different distances and pathways, thus providing information that cannot be obtained from a

269   single starting height (Cheng et al., 1993).

270   Previous studies suggest that there are increasing uncertainties as backward trajectory

271   distances increase (Stohl et al., 2002) and that PSCF modeling is prone to the trailing effect is

272   which locations upwind of sources are also identified as potential sources (Han et al., 2004).

273   An alternative to back trajectory calculations in the interpretation of atmospheric trace

274   substance measurements (Stohl et al., 2002) although this technique does not provide much

275   information on source locations.

276   Generally, PSCF results show that the potential sources covered wide areas instead of

277   indicating individual sources due to the trailing effect. The trailing effect appears since PSCF

278   distributes a constant weight along the path of the trajectories. To minimize the effect of

279   small n_{ij} (the number of trajectory segment endpoints that fall into the ij-th cell) values,

280   resulting in high TPSCF values with high uncertainties, an arbitrary weight function $W(n_{ij})$

281   was applied to down-weight the PSCF values for the cell in which the total number of end

282   points was less than three times the average value of the end points (Choi et al., 2011; Heo et

283   al., 2009; Hopke et al., 1995; Polissar et al., 2001). The TPSCF value for a grid cell was

284   defined with following Eq. (4).

285

$$P(TPSCF_{ij}) = \frac{P(m_{ij})_{10m} + P(m_{ij})_{50m} + P(m_{ij})_{100m}}{P(n_{ij})_{10m} + P(n_{ij})_{50m} + P(n_{ij})_{100m}} \times W \qquad (4)$$

287

288   where,

289
$$W(n_{ij}) = \begin{cases} 1.0, & 3n_{ave} < n_{ij} \\ 0.8, & 2n_{ave} < n_{ij} \leq 3n_{ave} \\ 0.6, & n_{ave} < n_{ij} \leq 2n_{ave} \\ 0.4, & 0.5n_{ave} < n_{ij} \leq n_{ave} \\ 0.2, & n_{ij} \leq 0.5n_{ave} \end{cases}$$

290

291   **4. Clean Air Policy Support System (CAPSS) data**

292   In this study, the Korean National Emission Inventory estimated using Clean Air Policy

293   Support System (CAPSS) data developed by the National Institute of Environmental

294   Research (NIER) were used (http://airemiss.nier.go.kr/main.jsp (accessed December 09,

295   2015)). The CAPSS is the national emission inventory system for the air pollutants (CO,

296   NOx, SOx, TSP, PM$_{10}$, PM$_{2.5}$, VOCs and NH$_3$) which utilizes various national, regional and

297   local statistical data collected from about 150 organizations in Korea. In CAPSS, the Source

298   Classification Category (SCC) excluding fugitive dust and biomass burning based on the

299   European Environment Agency's (EEA) CORe Inventory of AIR emissions was classified

300   into the following four levels (EMEP/CORINAIR) (NIER, 2011).

301   (1) The upper level (SCC1): 11 source categories ,

302   (2) The intermediate level (SCC2): 42 source categories and

303   (3) The lower level (SCC3): 173 source categories

13

304

305   The sectoral contributions of emissions of South Korea, Gyeongsangbuk-do and Pohang

306   for CO, NOx, SOx, TSP, PM_{10}, $PM_{2.5}$, VOC and NH_3 are shown in Fig. S2 (See SI for

307   details).

308   More detailed information about SCCs in CAPSS is described in Table S1.

309

310   **5.   Results and Discussions**

311   *5.1. General characteristics of TGM*

312   The seasonal distributions of TGM were characterized by large variability during each

313   sampling period (Fig. 2). The average concentration of TGM during the complete sampling

314   period was 5.0 ± 4.7 ng m^{-3} (range: 1.0-79.6 ng m^{-3}). This is significantly higher than the

315   Northern Hemisphere background concentration (~1.5 ng m^{-3}) (Sprovieri et al., 2010) and

316   those measured in China, in Japan and other locations in Korea, however lower than those

317   measured at Changchun, Gui Yang and Nanjing in China (Table 1). The median TGM

318   concentration was 3.6 ng m^{-3} which was much lower than that of the average, suggesting that

319   there were some extreme pollution episodes with very high TGM concentrations.

320   The TGM concentration follows a typical log-normal distribution (Fig. S3). The range of 2

321   to 5 ng m^{-3} dominated the distribution, accounting for more than half of the total number of

322   samples (60.8%). The maximum frequency of 28.1% occurred between 2 and 3 ng m^{-3}.

323   Extremely high TGM concentration events (>20 ng m^{-3}) were also observed (1.7% of the

324   time).

325

326

327

14

328   *5.2. Seasonal variations*

329   The TGM concentration was statistically significantly higher in fall (6.7 ± 6.4 ng m^{-3}) ($p <$

330   0.01), followed by spring (4.8 ± 4.0 ng m^{-3}), winter (4.5 ± 3.2 ng m^{-3}) and summer (3.8 ± 3.9

331   ng m^{-3}) (Table 2). The highest concentrations (TGM > 10 ng m^{-3}) were measured more

332   frequently in fall (24.7%), and the lowest concentrations (TGM < 3 ng m^{-3}) mainly occurred

333   in summer (49.7%). The low TGM concentration in summer is likely because increased

334   mixing height (Friedli et al., 2011), and gas phase oxidation (Choi et al., 2013; Huang et al.,

335   2010; Lynam and Keeler, 2006) at higher temperatures particularly at this sampling site

336   which is close to the ocean (2 km) where oxidation involving halogens may be enhanced

337   (Holmes et al., 2009; Lin et al., 2006). The high TGM concentrations in fall was due to

338   different wind direction (see Fig. S1), sources, relationships with other pollutants and

339   meteorological conditions. More detailed information can be found in Section 5.4.

340   The average concentrations of NO_2, O_3, CO, PM_{10} and SO_2 during the complete sampling

341   period were 23.1 ± 10.8 ppbv, 24.6 ± 12.5 ppbv, 673.7 ± 487.3 ppbv, 55.5 ± 26.4 μg m^{-3} and

342   6.7 ± 4.3 ppbv, respectively. NO_2, O_3, CO, PM_{10} and SO_2 concentrations were highest in

343   spring (Table 2). There was a statistically significant positive correlation between the TGM

344   and PM_{10} (r = 0.10) ($p < 0.01$). However, the TGM concentration was not significantly

345   correlated with NO_2, CO or SO_2 concentrations, suggesting that combustion associated with

346   space heating was not a significant source of TGM (Choi et al., 2009).

347

348   *5.3. Relationship between TGM and CO*

349   CO has a significant anthropogenic source and is considered to be an indicator of

350   anthropogenic emissions (Mao et al., 2008). Previous studies reported that TGM and CO

351   have a strong correlation because they have similar emission sources (combustion processes)

352   and similar long atmospheric residence times (Weiss-Penzias et al., 2003).

353   There was a weak positive correlation between TGM and CO in this study (r = 0.04) (p =

354   0.27). However there was a statistically significant correlation between TGM and CO in

355   winter (r = 0.25) ($p < 0.05$), suggesting that TGM and CO were affected by similar, possibly

356   distant, anthropogenic emission sources in winter.

357   On the other hand, there were no statistically significant correlations between TGM and

358   CO in spring (r = 0.02) (*$p = 0.78$*), in summer (r = 0.13) (*$p = 0.08$*), or in fall (r = -0.03) (*$p =$*

359   *0.69*), indicating that TGM and CO were affected by different anthropogenic emission

360   sources in these seasons.

361   Previous studies identified the long-range transport of mercury using the ΔTGM/ΔCO

362   enhancement ratio (Choi et al., 2009; Jaffe et al., 2005; Kim et al., 2009; Weiss-Penzias et al.,

363   2003; Weiss-Penzias et al., 2006). Kim et al. (2009) and Choi et al. (2009) investigated high

364   concentration events which were defined as at least a 10 h period with hourly average TGM

365   and CO concentrations higher than the average monthly TGM and CO concentrations. They

366   reported that long-range transport events were characterized by high values of TGM/CO ratio

367   (ΔTGM/ΔCO) (0.0052-0.0158 ng m^{-3} ppb^{-1}) and high correlations (r^2>0.5), whereas local

368   events showed low ΔTGM/ΔCO (0.0005 ng m^{-3} ppb^{-1} in average) and weak correlations (r$^2 <$

369   0.5).

370   The observed ΔTGM/ΔCO was 0.0001 ng m^{-3} ppb^{-1} in spring, 0.0005 ng m^{-3} ppb^{-1} in

371   summer, -0.0007 ng m^{-3} ppb^{-1} in fall, 0.0011 ng m^{-3} ppb^{-1} in winter, which are significantly

372   lower than that indicative of Asian long-range transport (0.0046-0.0056 ng m^{-3} ppb^{-1}) (Friedli

16

373   et al., 2004; Jaffe et al., 2005; Weiss-Penzias et al., 2006), suggesting that local sources are

374   more important than that of long-range transport in this study. The ΔTGM/ΔCO in winter

375   (0.0011 ng m^{-3} ppb^{-1}) was similar to that of a site impacted by local sources in Korea (Kim et

376   al., 2009) and in US industrially related events (0.0011 ng m^{-3} ppb^{-1}) (Weiss-Penzias et al.,

377   2007).

378   There are also uncertainties from the potential mixing between Hg associated with long-

379   range transported airflows and local air making it difficult to distinguish between distant and

380   local source impacts. However, it is possible that the one-week sampling period in each

381   season did not capture the long-range transport events, and more can be learned using a larger

382   dataset than just using the one-week sampling period to confirm these results.

383

384   *5.4. Diurnal variations*

385   Diurnal variations of TGM (Fig. 3), co-pollutants concentrations, and meteorological

386   data were observed (Fig. S4). TGM, O_3, CO, SO_2, and temperature in the daytime (06:00-

387   18:00) were higher than those in the nighttime (18:00-06:00) ($p < 0.05$) except PM_{10} ($p =$

388   0.09) (Fig. S5). However, NO_2 during the nighttime because of relatively lower

389   photochemical reactivity with O_3 was higher than that in daytime ($p < 0.05$) (Adame et al.,

390   2012).

391   The daytime TGM concentration (5.3 ± 4.7 ng m^{-3}) was higher than that in the nighttime

392   (4.7 ± 4.7 ng m^{-3}) ($p < 0.01$), which was similar to several previous studies (Cheng et al.,

393   2014; Gabriel et al., 2005; Nakagawa, 1995; Stamenkovic et al., 2007) but different than

394   another studies (Lee et al., 1998). Previous studies reported that this different is due to local

395   sources close to the sampling site (Cheng et al., 2014; Gabriel et al., 2005), a positive

396   correlation between TGM concentration and ambient air temperature (Nakagawa, 1995) and

17

397   increased traffic (Stamenkovic et al., 2007). However, another study suggested that the higher

398   TGM concentration during the night was due to the shallowing of the boundary layer, which

399   concentrated the TGM near the surface (Lee et al., 1998).

400   In a previous study the daytime TGM concentration was relatively lower than that in the

401   nighttime because the sea breeze transported air containing low amounts of TGM from the

402   ocean during the daytime whereas the land breeze transported air containing relatively high

403   concentrations of TGM from an urban area during the nighttime (Kellerhals et al., 2003).

404   Although it is possible that the land-sea breeze may affect diurnal variations in TGM

405   concentrations since the sampling site was near the ocean and lower TGM were also observed

406   during the daytime, the higher concentrations in the daytime than those in nighttime were due

407   to local emission sources because the daytime temperature (14.7 ± 10.0 ºC) was statistically

408   significantly higher than that in the nighttime (13.0 ± 9.8 ºC) (t-test, $p < 0.05$) and there was a

409   weak but statistically significant negative correlation between TGM concentration and

410   ambient air temperature (r = -0.08) ($p < 0.05$). In addition, there are several known Hg

411   sources such as iron and steel manufacturing facilities including electric and sintering

412   furnaces using coking between the sampling site and the ocean.

413   As shown in Fig. 3 and Fig. S4, there was a weak but negative relationship between the

414   TGM concentrations and O_3 concentrations (r = -0.18) ($p < 0.01$), suggesting that oxidation

415   of GEM in the oxidizing atmosphere during periods of strong atmospheric mixing was

416   partially responsible for the diurnal variations of TGM concentrations. In addition, oxidation

417   of GEM by bromine species in the coastal area (Obrist et al., 2011) or by chloride radicals in

418   marine boundary layer (Laurier et al., 2003) might play a significant role. If oxidation of

419   GEM occurred, GOM concentrations would increase. However there are uncertainties on the

420   net effects on TGM (the sum of the GEM and the GOM) since we did not measure GOM

421   concentrations.

422   TGM concentration was negatively correlated with ambient air temperature *(r = -0.08)*

423   *(p < 0.05)* because high ambient air temperature in the daytime will increase the height of the

424   boundary layer and dilute the TGM, and the relatively lower boundary layer at nighttime

425   could concentrate the TGM in the atmosphere (Li et al., 2011). Although there was a

426   statistically significant negative correlation between the TGM concentration and ambient air

427   temperature, there was a rapid increase in TGM concentration between 06:00-09:00 when

428   ambient temperatures also increased possibly due to local emissions related to industrial

429   activities, increased traffic, and activation of local surface emission sources. Similar patterns

430   were found in previous studies (Li et al., 2011; Stamenkovic et al., 2007). Nonparametric

431   correlations revealed that there is a weak positive correlation between TGM and ambient air

432   temperature ($r_s = 0.11$, *p=0.27*) between 06:00-09:00. The TGM concentration was negatively

433   correlated with O_3 ($r_s = -0.33$, *p<0.01*) but positively correlated with NO_2 ($r_s = 0.21$, *p<0.05*),

434   suggesting that the increased traffic is the main source of TGM during these time periods.

435   Compared to other seasons, significantly different diurnal variations of TGM were

436   observed in fall. The daytime TGM concentrations in fall were similar to those in other

437   seasons, however, the nighttime TGM concentrations in fall were much higher than other

438   seasons. As described earlier in Section 5.2, the high TGM concentrations in fall was

439   possibly due to the relationship between other pollutants and meteorological conditions as

440   well as different wind direction and sources. The nighttime TGM concentrations in fall were

441   simultaneously positively correlated with PM_{10} (r=0.26) (*p<0.05*) and CO (r=0.21) (*p<0.05*)

442   concentrations and wind speed (r=0.35) (*p<0.01*), suggesting that the combustion process is

443   an important source during this period.

19

444   TGM generally showed a consistent increase in the early morning (06:00-09:00) and a

445   decrease in the afternoon (14:00-17:00), similar to previous studies (Dommergue et al., 2002;

446   Friedli et al., 2011; Li et al., 2011; Liu et al., 2011; Mao et al., 2008; Shon et al., 2005; Song

447   et al., 2009; Stamenkovic et al., 2007). Significantly different diurnal patterns have been

448   observed at many suburban sites with the daily maximum occurring in the afternoon (12:00-

449   15:00), possibly due to local emission sources and transport (Fu et al., 2010; Fu et al., 2008;

450   Kuo et al., 2006; Wan et al., 2009). Other studies in Europe reported that TGM

451   concentrations were relatively higher early in the morning or at night possibly due to mercury

452   emissions from surface sources that accumulated in the nocturnal inversion layer (Lee et al.,

453   1998; Schmolke et al., 1999).

454   Based on the above results, the diurnal variations in TGM concentration are due to a

455   combination of: 1) reactions with an oxidizing atmosphere, 2) changes in ambient

456   temperature and 3) local emissions related to industrial activities. To supplement these

457   conclusions CPF and CBPF were used to identify source directions and TPSCF was used to

458   identify potential source locations.

459

460   *5.5. CPF, CBPF and TPSCF results of TGM*

461   Conventional CPF, CBPF and TPSCF plots for TGM concentrations higher than the

462   average concentration show high source probabilities to the west in the direction of large steel

463   manufacturing facilities and waste incinerators (Fig. 4). The CPF only shows high

464   probabilities from the west and provides no further information, however, the CBPF shows

465   groups of sources with the high probabilities from the west and the northeast. CBPF shows

466   that the high probabilities from the west occurred under high wind speed (> 3 m s^{-1})

467   indicative of emissions from stacks as well as low wind speed (≤ 3 m s^{-1}) indicative of non-

468   buoyant ground level sources (Uria-Tellaetxe and Carslaw, 2014).

469   As described in Section 5.3, correlations between TGM and CO revealed that TGM and

470   CO were affected by similar anthropogenic emission sources in winter but affected by

471   different sources in spring, summer and fall, which is supported by Fig. S6 which shows

472   significantly different seasonal patterns of CPF and CBPF for TGM concentrations.

473   However, compared to Fig. 4, the CPF and CBPF patterns in fall were similar to those during

474   the whole sampling periods. Especially, the nighttime TGM concentration in fall was

475   simultaneously positively correlated with PM$_{10}$ (r=0.26) ($p<0.05$) and CO (r=0.21) ($p<0.05$)

476   concentrations and wind speed (r=0.35) ($p<0.01$), indicating that the combustion process

477   from the west is an important source during this period.

478   Since TGM showed a significant correlation with CO (r=0.25) ($p<0.05$) and showed a

479   weak positive correlation with PM$_{10}$ (r=0.08) ($p=0.33$) in winter with high wind speed,

480   combustion sources from the west are likely partially responsible for this result.

481   TPSCF identified the likely sources of TGM as the iron and manufacturing facilities and

482   the hazardous waste incinerators which are located to the west from the sampling site. A

483   previous study reported that the waste incinerators (9%) and iron and steel manufacturing

484   (7%) were relatively high Hg emissions sources in Korea (Kim et al., 2010). Waste

485   incinerators emissions were due to the high Hg content in the waste (Lee et al., 2004).

486   Emissions from iron and steel manufacturing are due to the numerous electric and sintering

487   furnaces using coking which emits relatively high mercury concentrations (Lee et al., 2004)

488   in Gyeongsangbuk-do including Pohang. There are several coke plants around the sampling

489   site (http://www.poscoenc.com/upload/W/BUSINESS/PDF/ENG_PLANT_2_1_3_5.pdf

490   (accessed December 09, 2015)). They are essential parts of the iron and steel manufacturing,

491 and the major source of atmospheric mercury related to the iron and steel manufacturing is

492 from coke production (Pacyna et al., 2006).

493 The coastal areas east of the sampling site where there are large ports were also identified

494 as the likely source areas of TGM. A previous study reported that the emissions of gaseous

495 and particulate pollutants were high during vehicular operations in port areas and from

496 marine vessel and launches (Gupta et al., 2002). Another possibility is that significant amount

497 of GEM are emitted from the ocean surface because of photo-chemically and

498 microbiologically mediated photo-reduction of dissolved GOM (Amyot et al., 1994; Zhang

499 and Lindberg, 2001). The northeast direction including the East Sea was also identified as

500 potential source areas likely because this is an area with lots of domestic passenger ships

501 routes. The south from the sampling site was also identified as a likely source area of TGM

502 where Ulsan Metropolitan City, South Korea's seventh largest metropolis with a population

503 of over 1.1 million is located. It includes a large petrochemical complex known as a TGM

504 source (Jen et al., 2013).

505

506 **Conclusions**

507   During the sampling periods, the average TGM concentration was higher than the Northern

508   Hemisphere background concentration, however, considerably lower than those near urban

509   areas in China and higher than those in Japan and other locations in Korea. The median

510   concentration of TGM was much lower than that of the average, suggesting that there were

511   some extreme pollution episodes with very high TGM concentrations. The TGM

512   concentration was highest in fall, followed by spring, winter and summer. The high TGM

513   concentration in fall is due to transport from different wind directions than during the other

514   periods. The low TGM concentration in summer is likely due to increased mixing height and

515   gas phase oxidation at higher temperatures particularly at this sampling site which is close to

516   the ocean (2 km) where oxidation involving halogens may be enhanced.

517   TGM consistently showed a diurnal variation with a maximum in the early morning

518   (06:00-09:00) and minimum in the afternoon (14:00-17:00). Although there was a statistically

519   significant negative correlation between the TGM concentration and ambient air temperature,

520   the daytime TGM concentration was higher than those in the nighttime, suggesting that local

521   emission sources are important. There was a negative relationship between the TGM

522   concentrations and O_3 concentrations, indicating that the oxidation was partially responsible

523   for the diurnal variations of TGM concentrations. The observed $\Delta TGM/\Delta CO$ was

524   significantly lower than that indicative of Asian long-range transport, suggesting that local

525   sources are more important than that of long-range transport. CPF only shows high

526   probabilities to the west from the sampling site where there are large steel manufacturing

527   facilities and waste incinerators. However, CBPF and TPSCF indicated that the dominant

528   sources of TGM were the hazardous waste incinerators and the coastal areas in the northeast

529   as well as the iron and manufacturing facilities in the west. The domestic passenger ships

530   routes in the East Sea were also identified as possible source areas.

531

532   **Author contribution**

533   Yong-Seok Seo conducted a design of the study, the experiments and analysis of data, wrote

534   the initial manuscript, and finally approved the final manuscript. Seung-Pyo Jeong, Eun Ha

535   Park, Tae Young Kim, Hee-Sang Eum, Dae Gun Park, Eunhye Kim, Jaewon Choi and Jeong-

536   Hun Kim conducted the experiments, analysis of data, and finally approved the final

537   manuscript. Thomas M. Holsen, Young-Ji Han and Eunhwa Choi and Soontae Kim

538   conducted interpretation of the results, revision of the initial manuscript, and finally approved

539   the final manuscript. Seung-Muk Yi conducted a design of the study, acquisition of data of the

540   study, interpretation of data, and revision of the initial manuscript, and finally approved the final

541   manuscript.

542

543   **Acknowledgments**

549

550 **Table List**

551 Table 1. Comparison with previous studies for TGM concentrations.

552 Table 2. Summary of atmospheric concentrations of TGM and co-pollutants, and

553 meteorological data.

554

555 **Figure List**

556 Fig. 1. The location of sampling site in this study ((a) South Korea, (b) Gyeongsangbuk-do

557 and (c) Pohang).

558 Fig. 2. Time-series of TGM concentrations in this study.

559 Fig. 3. The diurnal variations of TGM concentrations during the sampling periods.

560 Fig. 4. CPF, CBPF and TPSCF plots for TGM higher than average concentration.

561   **Table 1.** Comparison with previous studies for TGM concentrations.

Country	Location	Sampling period	TGM conc. (ng m^{-3})	Classifications	Reference
China	Mt. Hengduan, Qinghai–Tibet Plateau	Jul. 2010 ~ Oct. 2010	2.5	Remote	Fu et al. (2015)
China	Nanjing, Jiangsu	Jan. 2011 ~ Oct. 2011	7.9	Urban	Hall et al. (2014)
China	Mt. Dinghu, Guangdong	Oct. 2009 ~ Apr. 2010	5.1	Rural	Chen et al. (2013)
China	Guangzhou, Guangdong	Nov. 2010 ~ Nov. 2011	4.6	Urban	Chen et al. (2013)
China	Gui Yang, Guizhou	Jan. 2010 ~ Feb. 2010	8.4	Urban	Feng et al. (2004)
China	Changchun, Jilin	Jul. 1999 ~ Jul. 2000	13.5-25.4	Urban	Fang et al. (2004)
Japan	Fukuoka	Jun. 2012 ~ May 2013	2.33	Urban	Marumoto et al. (2015)
Japan	Tokai-mura	Oct. 2005 ~ Aug. 2006	3.8	Suburban	Osawa et al. (2007)
Japan	Tokyo	Apr. 2000 ~ Mar. 2001	2.7	Urban	Sakata and Marumoto (2002)
Korea	Seoul	1987 ~ 2013	3.7	Urban	Kim et al. (2016)
Korea	Gangwon-do, Chuncheon	2006 ~ 2009	2.1	Rural	Han et al. (2014)
Korea	Seoul	Feb. 2005 ~ Feb. 2006	3.2	Urban	Kim et al. (2009)
Korea	Seoul	Feb. 2005 ~ Dec. 2006	3.4	Urban	Choi et al. (2009)
Korea	Seoul	19 Sep. 1997 ~ 29 Sep. 1997 27 May. 1998 ~ 18 Jun. 1998	3.6	Urban	Kim and Kim (2001)
Korea	Gyeongsangbuk-do, Pohang	17 Aug. 2012 ~ 23 Aug. 2012 9 Oct. 2012 ~ 17 Oct. 2012 22 Jan. 2013 ~ 29 Jan. 2013 26 Mar. 2013 ~ 3 Apr. 2013	5.0	Urban	This study

562

26

563 **Table 2.** Summary of atmospheric concentrations of TGM and co-pollutants, and meteorological data. Note that TGM was measured every 5-
564 min, and other pollutants and meteorological data were measured every 1-hour.

|		TGM (ng m^{-3})	NO$_2$ (ppb)	O$_3$ (ppb)	CO (ppb)	PM$_{10}$ (µg m^{-3})	SO$_2$ (ppb)	Temperature (℃)	Wind speed (m s^{-1})	Humidity (%)	Solar radiation (MJ m^{-2})
Spring	N	2139	189	215	215	215	215	216	216	216	216
	Average	4.8 ± 4.0	25.3 ± 9.0	29.4 ± 14.2	766.5 ± 505.2	70.1 ± 26.0	7.6 ± 3.8	10.5 ± 4.2	2.2 ± 1.2	56.2 ± 16.8	0.82 ± 1.09
	Range	1.9 – 45.3	8 – 55	2 – 58	300 – 3100	28 - 204	5 - 35	1.1 – 21.6	0.4 – 6.2	19.0 – 94.0	0 – 3.44
Summer	N	1863	187	188	187	188	188	186	180	186	141
	Average	3.8 ± 3.9	18.3 ± 9.2	18.9 ± 10.1	697.3 ± 689.7	35.1 ± 15.8	6.5 ± 6.2	26.6 ± 4.2	2.2 ± 1.1	82.5 ± 13.9	0.40 ± 0.69
	Range	1.2 – 75.9	4 – 44	5 – 48	200 – 3300	12 – 87	2 - 27	19.7 – 34.1	0.1 – 6.4	43 - 98	0 – 2.92
Fall	N	2226	212	212	212	212	211	216	216	216	216
	Average	6.7 ± 6.4	25.0 ± 7.8	23.7 ± 13.1	662.7 ± 350.2	58.1 ± 17.8	5.3 ± 3.5	17.4 ± 3.2	2.1 ± 0.8	54.5 ± 14.7	0.62 ± 0.90
	Range	1.0 – 79.6	9 – 53	6 – 69	300 – 2900	20 - 145	3 - 39	11.7 – 25.2	0.5 – 4.5	12 - 79	0 – 2.90
Winter	N	1917	188	187	188	188	186	192	192	192	192
	Average	4.5 ± 3.2	23.5 ± 14.7	26.1 ± 8.7	556.4 ± 298.9	56.3 ± 30.5	7.4 ± 2.5	1.1 ± 4.3	2.8 ± 1.1	46.3 ± 24.5	0.43 ± 0.71
	Range	1.3 – 66.4	5 – 74	1 – 41	200 – 2400	18 – 161	5 – 24	-0.65 – 10.1	0.5 – 6.0	11 - 90	0 – 2.34
Total	N	8145	776	802	802	803	800	810	804	810	765
	Average	5.0 ± 4.7	23.1 ± 10.8	24.6 ± 12.5	673.7 ± 487.3	55.5 ± 26.4	6.7 ± 4.3	13.8 ± 9.9	2.3 ± 1.1	59.4 ± 22.1	0.59 ± 0.90
	Range	1.0 – 79.6	4 – 74	1 – 69	200 – 3300	12 – 204	2 – 39	-6.5 – 34.1	0.1 – 6.4	11 - 98	0 – 3.44

565
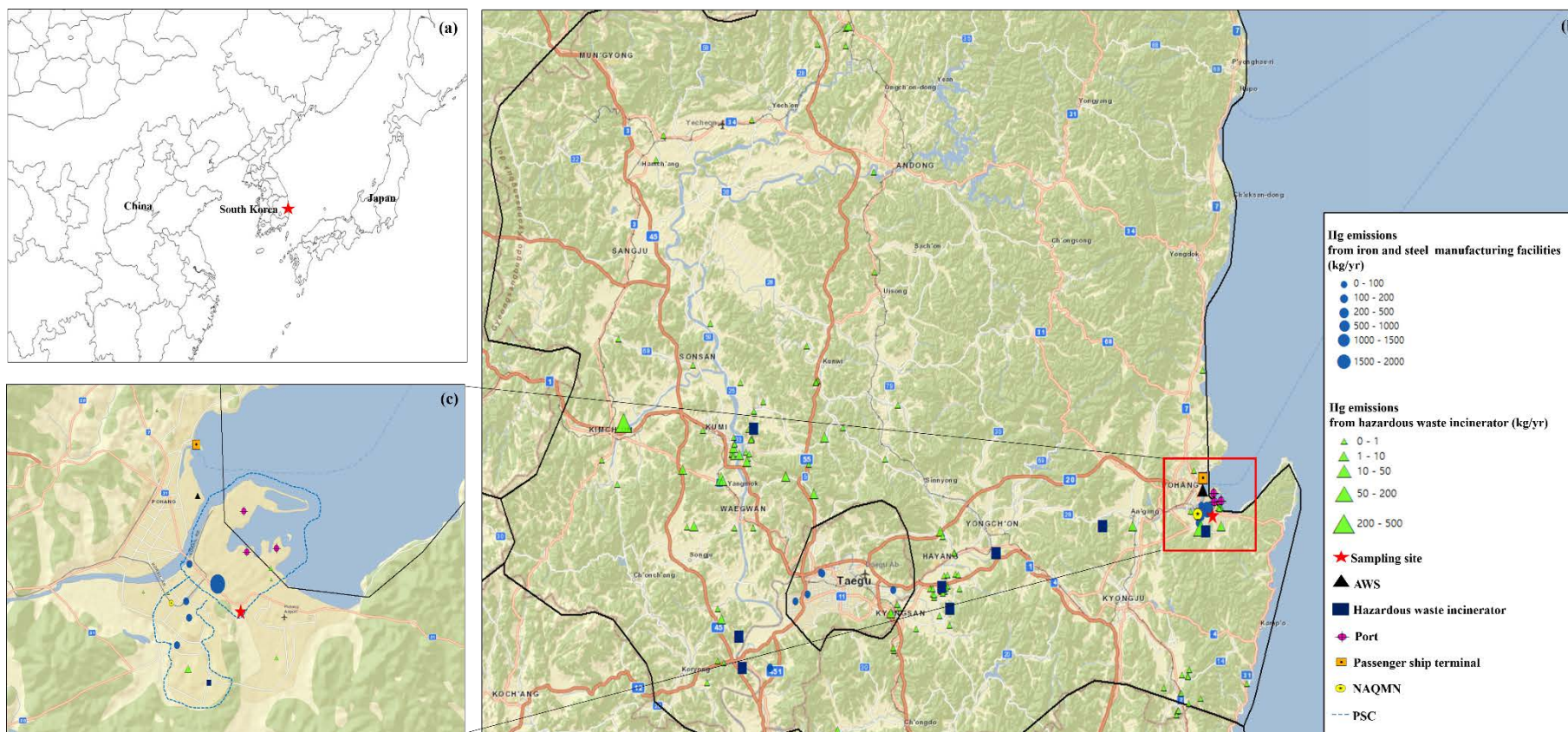
Fig. 1. The location of sampling site in this study ((a) South Korea, (b) Gyeongsangbuk-do and (c) Pohang). AWS, NAQMN and PSC represent Automatic Weather Station, National Air Quality Monitoring Network and Pohang Steel Complex, respectively.
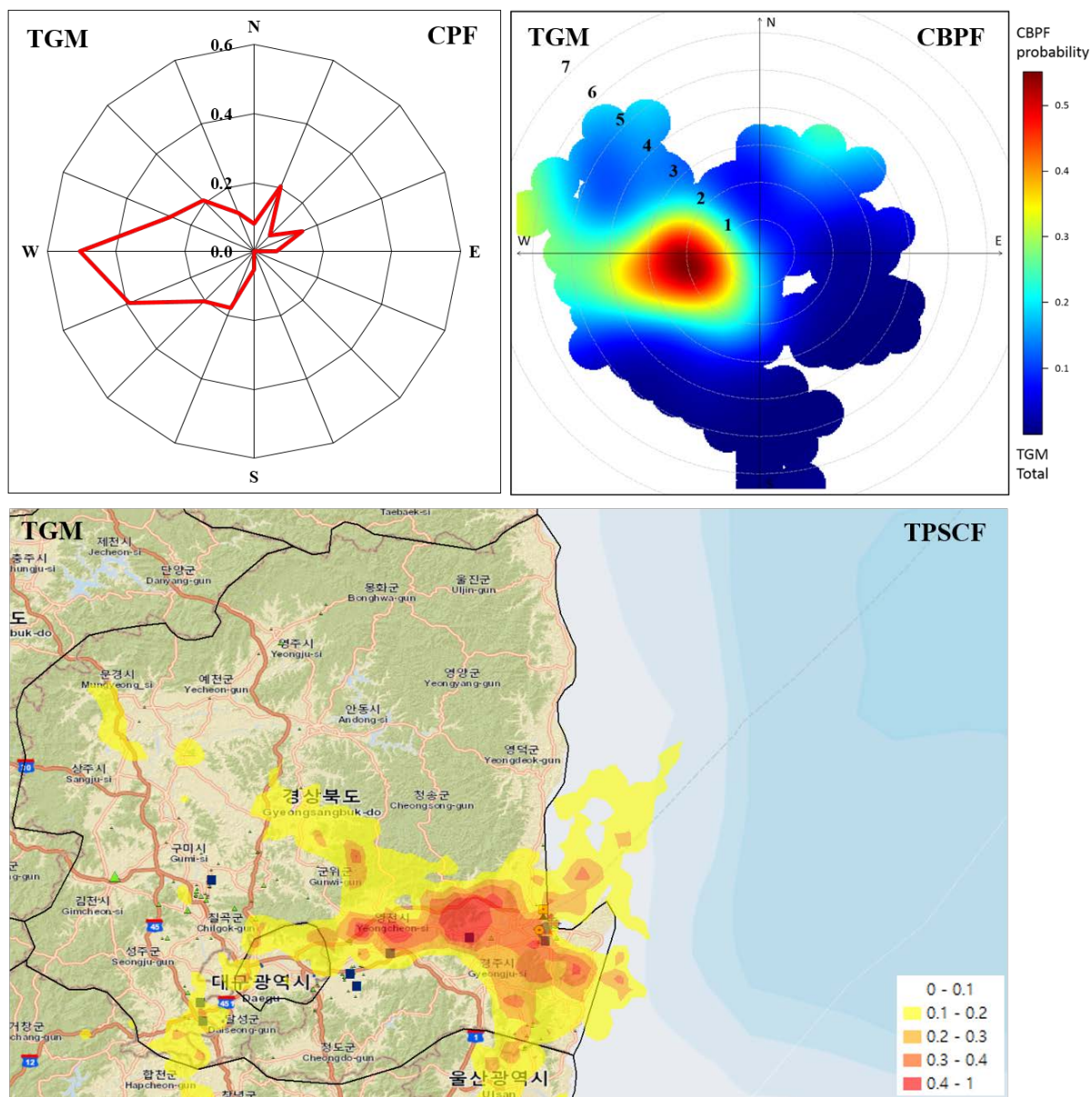
566
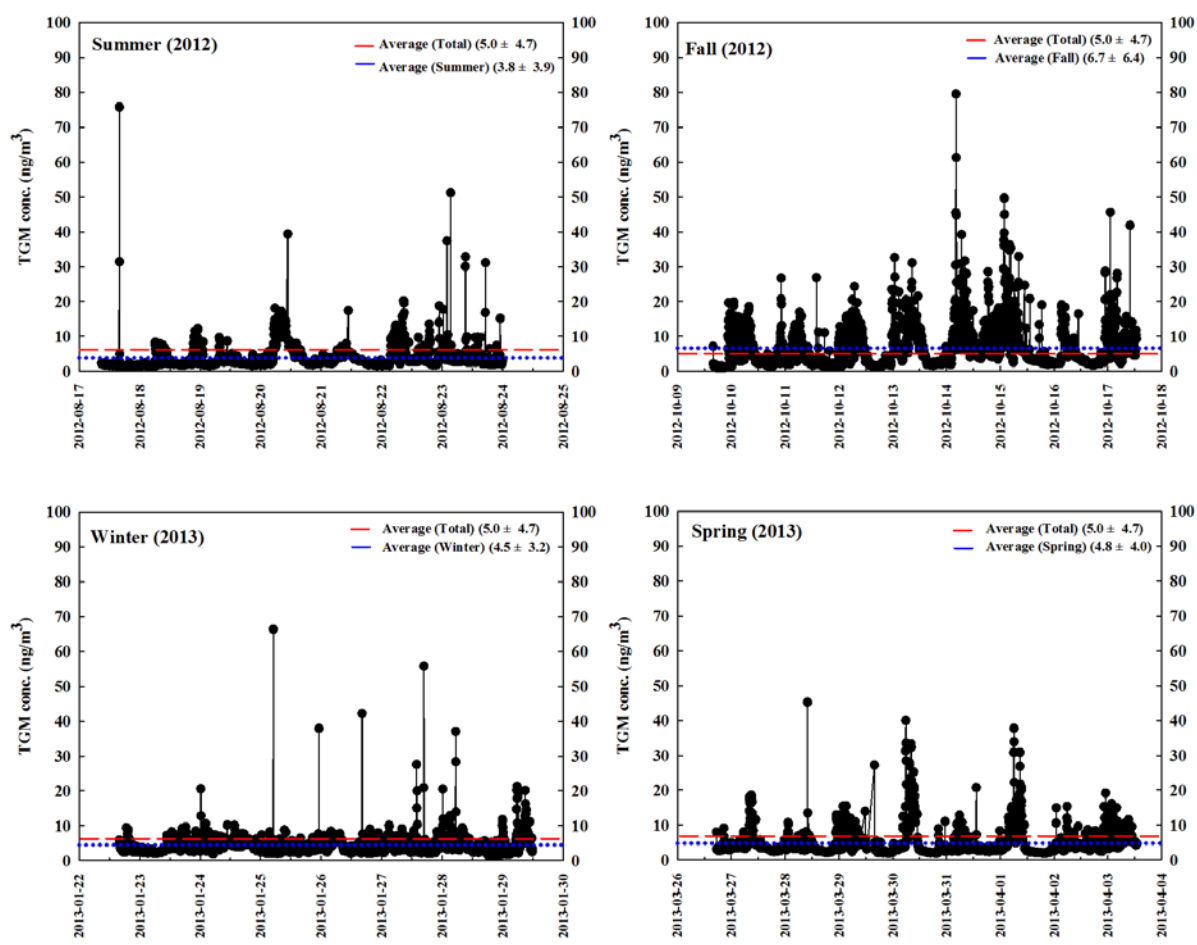
567

568   **Fig. 2.** Time-series of TGM concentrations in this study.
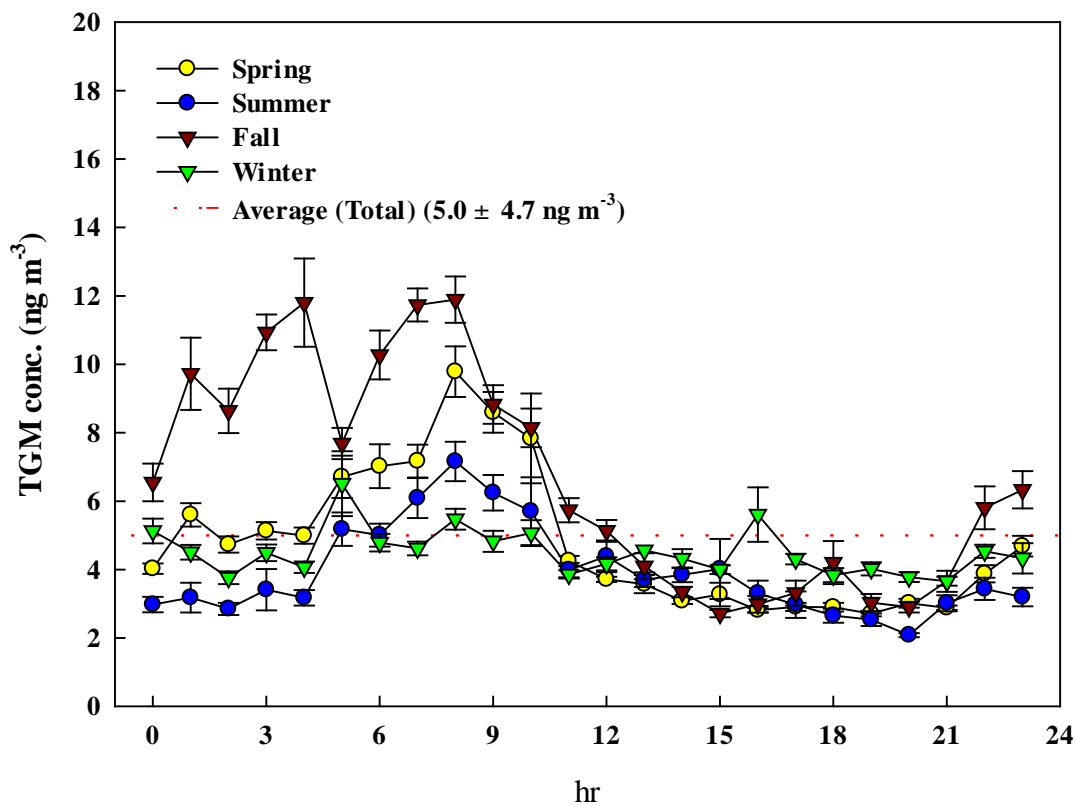
569
570   **Fig. 3.** The diurnal variations of TGM concentrations during the sampling periods.
571   The error bars represent standard error.

Fig. 4. CPF, CBPF and TPSCF plots for TGM higher than average concentration. The radial axes of CPF and CBPF are the probability and the wind speed (m s^{-1}), respectively.

References

Adame, J., Notario, A., Villanueva, F., and Albaladejo, J.: Application of cluster analysis to surface ozone, NO_2 and SO_2 daily patterns in an industrial area in Central-Southern Spain measured with a DOAS system, Sci. Total Environ., 429, 281-291, 2012.

Amap/Unep. Technical Background Report for the Global Mercury Assessment 2013. UNEP Chemicals Branch Geneva, Switzerland. 2013.

Amyot, M., Mcqueen, D. J., Mierle, G., and Lean, D. R.: Sunlight-induced formation of dissolved gaseous mercury in lake waters, Environ. Sci. Technol., 28, 2366-2371, 1994.

Ashbaugh, L. L., Malm, W. C., and Sadeh, W. Z.: A residence time probability analysis of sulfur concentrations at Grand Canyon National Park, Atmospheric Environment (1967), 19, 1263-1270, 1985.

Begum, B. A., Kim, E., Biswas, S. K., and Hopke, P. K.: Investigation of sources of atmospheric aerosol at urban and semi-urban areas in Bangladesh, Atmos. Environ., 38, 3025-3038, 2004.

Brown, R. J., Goddard, S. L., Butterfield, D. M., Brown, A. S., Robins, C., Mustoe, C. L., and Mcghee, E. A.: Ten years of mercury measurement at urban and industrial air quality monitoring stations in the UK, Atmos. Environ., 109, 1-8, 2015.

Bullock, O. R., Brehme, K. A., and Mapp, G. R.: Lagrangian modeling of mercury air emission, transport and deposition: an analysis of model sensitivity to emissions uncertainty, Sci. Total Environ., 213, 1-12, 1998.

Chen, L., Liu, M., Xu, Z., Fan, R., Tao, J., Chen, D., Zhang, D., Xie, D., and Sun, J.: Variation trends and influencing factors of total gaseous mercury in the Pearl River Delta—A highly industrialised region in South China influenced by seasonal monsoons, Atmos. Environ., 77, 757-766, 2013.

Cheng, I., Zhang, L., Mao, H., Blanchard, P., Tordon, R., and Dalziel, J.: Seasonal and diurnal patterns of speciated atmospheric mercury at a coastal-rural and a coastal-urban site, Atmos. Environ., 82, 193-205, 2014.

Cheng, M. D., Hopke, P. K., and Zeng, Y.: A receptor-oriented methodology for determining source regions of particulate sulfate observed at Dorset, Ontario, Journal of Geophysical Research: Atmospheres (1984–2012), 98, 16839-16849, 1993.

Choi, E.-M., Kim, S.-H., Holsen, T. M., and Yi, S.-M.: Total gaseous concentrations in mercury in Seoul, Korea: local sources compared to long-range transport from China and Japan, Environ. Pollut., 157, 816-822, 2009.

Choi, E., Heo, J.-B., Hopke, P. K., Jin, B.-B., and Yi, S.-M.: Identification, apportionment, and photochemical reactivity of non-methane hydrocarbon sources in Busan, Korea, Water, Air, Soil Pollut., 215, 67-82, 2011.

Choi, H.-D., Huang, J., Mondal, S., and Holsen, T. M.: Variation in concentrations of three mercury (Hg) forms at a rural and a suburban site in New York State, Sci. Total Environ., 448, 96-106, 2013.

Dommergue, A., Ferrari, C. P., Planchon, F. A., and Boutron, C. F.: Influence of anthropogenic sources on total gaseous mercury variability in Grenoble suburban air (France), Sci. Total Environ., 297, 203-213, 2002.

Durnford, D., Dastoor, A., Figueras-Nieto, D., and Ryjkov, A.: Long range transport of mercury to the Arctic and across Canada, Atmospheric Chemistry and Physics, 10, 6063-6086, 2010.

Dvonch, J., Graney, J., Marsik, F., Keeler, G., and Stevens, R.: An investigation of source–receptor relationships for mercury in south Florida using event precipitation data, Sci. Total Environ., 213, 95-108, 1998.

Ebinghaus, R., Jennings, S., Kock, H., Derwent, R., Manning, A., and Spain, T.: Decreasing trends in total gaseous mercury observations in baseline air at Mace Head, Ireland from 1996 to 2009, Atmos. Environ., 45, 3475-3480, 2011.

Fang, F., Wang, Q., and Li, J.: Urban environmental mercury in Changchun, a metropolitan city in Northeastern China: source, cycle, and fate, Sci. Total Environ., 330, 159-170, 2004.

Feng, X., Shang, L., Wang, S., Tang, S., and Zheng, W.: Temporal variation of total gaseous mercury in the air of Guiyang, China, Journal of Geophysical Research: Atmospheres (1984–2012), 109, 2004.

Flanders, J., Turner, R., Morrison, T., Jensen, R., Pizzuto, J., Skalak, K., and Stahl, R.: Distribution, behavior, and transport of inorganic and methylmercury in a high gradient stream, Appl. Geochem., 25, 1756-1769, 2010.

Friedli, H., Arellano Jr, A., Geng, F., Cai, C., and Pan, L.: Measurements of atmospheric mercury in Shanghai during September 2009, Atmos. Chem. Phys., 11, 3781-3788, 2011.

Friedli, H. R., Radke, L. F., Prescott, R., Li, P., Woo, J. H., and Carmichael, G. R.: Mercury in the atmosphere around Japan, Korea, and China as observed during the 2001 ACE-Asia field campaign: Measurements, distributions, sources, and implications, Journal of Geophysical Research: Atmospheres (1984–2012), 109, 2004.

Fu, X., Feng, X., Dong, Z., Yin, R., Wang, J., Yang, Z., and Zhang, H.: Atmospheric gaseous elemental mercury (GEM) concentrations and mercury depositions at a high-altitude mountain peak in south China, Atmos. Chem. Phys., 10, 2425-2437, 2010.

Fu, X., Feng, X., Zhu, W., Wang, S., and Lu, J.: Total gaseous mercury concentrations in ambient air in the eastern slope of Mt. Gongga, South-Eastern fringe of the Tibetan plateau, China, Atmos. Environ., 42, 970-979, 2008.

Fu, X., Zhang, H., Lin, C.-J., Feng, X., Zhou, L., and Fang, S.: Correlation slopes of GEM/CO, GEM/CO 2, and GEM/CH 4 and estimated mercury emissions in China, South Asia, the Indochinese Peninsula, and Central Asia derived from observations in northwestern and southwestern China, Atmos. Chem. Phys., 15, 1013-1028, 2015.

Gabriel, M. C., Williamson, D. G., Brooks, S., and Lindberg, S.: Atmospheric speciation of mercury in two contrasting Southeastern US airsheds, Atmos. Environ., 39, 4947-4958, 2005.

Gauchard, P.-A., Ferrari, C. P., Dommergue, A., Poissant, L., Pilote, M., Guehenneux, G., Boutron, C. F., and Baussand, P.: Atmospheric particle evolution during a nighttime atmospheric mercury depletion event in sub-Arctic at Kuujjuarapik/Whapmagoostui, Quebec, Canada, Sci. Total Environ., 336, 215-224, 2005.

Gupta, A., Patil, R., and Gupta, S.: Emissions of gaseous and particulate pollutants in a port and harbour region in India, Environ. Monit. Assess., 80, 187-205, 2002.

Hall, C. B., Mao, H., Ye, Z., Talbot, R., Ding, A., Zhang, Y., Zhu, J., Wang, T., Lin, C.-J., and Fu, C.: Sources and Dynamic Processes Controlling Background and Peak Concentrations of TGM in Nanjing, China, Atmosphere, 5, 124-155, 2014.

Han, Y.-J., Holsen, T. M., Hopke, P. K., Cheong, J.-P., Kim, H., and Yi, S.-M.: Identification of source locations for atmospheric dry deposition of heavy metals during yellow-sand events in Seoul, Korea in 1998 using hybrid receptor models, Atmos. Environ., 38, 5353-5361, 2004.

671 Han, Y.-J., Holsen, T. M., Hopke, P. K., and Yi, S.-M.: Comparison between back-trajectory
672   based modeling and Lagrangian backward dispersion modeling for locating sources of
673   reactive gaseous mercury, Environ. Sci. Technol., 39, 1715-1723, 2005.
674 Han, Y.-J., Kim, J.-E., Kim, P.-R., Kim, W.-J., Yi, S.-M., Seo, Y.-S., and Kim, S.-H.:
675   General trends of atmospheric mercury concentrations in urban and rural areas in
676   Korea and characteristics of high-concentration events, Atmos. Environ., 94, 754-764,
677   2014.
678 Heo, J.-B., Hopke, P., and Yi, S.-M.: Source apportionment of PM2.5 in Seoul, Korea, Atmos.
679   Chem. Phys., 9, 4957-4971, 2009.
680 Holmes, C. D., Jacob, D. J., Mason, R. P., and Jaffe, D. A.: Sources and deposition of
681   reactive gaseous mercury in the marine atmosphere, Atmos. Environ., 43, 2278-2285,
682   2009.
683 Hopke, P., Barrie, L., Li, S. M., Cheng, M. D., Li, C., and Xie, Y.: Possible sources and
684   preferred pathways for biogenic and non-sea-salt sulfur for the high Arctic, Journal of
685   Geophysical Research: Atmospheres (1984–2012), 100, 16595-16603, 1995.
686 Hopke, P. K.: Recent developments in receptor modeling, J. Chemometrics, 17, 255-265,
687   2003.
688 Hopke, P. K., Zhou, L., and Poirot, R. L.: Reconciling trajectory ensemble receptor model
689   results with emissions, Environ. Sci. Technol., 39, 7980-7983, 2005.
690 Hoyer, M., Burke, J., and Keeler, G. 1995. Atmospheric sources, transport and deposition of
691   mercury in Michigan: two years of event precipitation. *Mercury as a Global*
692   *Pollutant.* Springer.
693 Hsu, Y.-K., Holsen, T. M., and Hopke, P. K.: Comparison of hybrid receptor models to locate
694   PCB sources in Chicago, Atmos. Environ., 37, 545-562, 2003.
695 Huang, J., Choi, H.-D., Hopke, P. K., and Holsen, T. M.: Ambient mercury sources in
696   Rochester, NY: results from principle components analysis (PCA) of mercury
697   monitoring network data, Environ. Sci. Technol., 44, 8441-8445, 2010.
698 Jaffe, D., Prestbo, E., Swartzendruber, P., Weiss-Penzias, P., Kato, S., Takami, A.,
699   Hatakeyama, S., and Kajii, Y.: Export of atmospheric mercury from Asia, Atmos.
700   Environ., 39, 3029-3038, 2005.
701 Jen, Y.-H., Yuan, C.-S., Hung, C.-H., Ie, I.-R., and Tsai, C.-M.: Tempospatial variation and
702   partition of atmospheric mercury during wet and dry seasons at sensitivity sites within
703   a heavily polluted industrial city, Aerosol Air Qual. Res, 13, 13-23, 2013.
704 Keeler, G., and Barres, J.: Sampling and Analysis for Atmospheric Mercury, Center for
705   Environmental Research Information, Cincinati, 1999.
706 Kellerhals, M., Beauchamp, S., Belzer, W., Blanchard, P., Froude, F., Harvey, B., Mcdonald,
707   K., Pilote, M., Poissant, L., and Puckett, K.: Temporal and spatial variability of total
708   gaseous mercury in Canada: results from the Canadian Atmospheric Mercury
709   Measurement Network (CAMNet), Atmos. Environ., 37, 1003-1011, 2003.
710 Kim, E., Hopke, P. K., and Edgerton, E. S.: Source identification of Atlanta aerosol by
711   positive matrix factorization, J. Air Waste Manage. Assoc., 53, 731-739, 2003a.
712 Kim, E., Larson, T. V., Hopke, P. K., Slaughter, C., Sheppard, L. E., and Claiborn, C.: Source
713   identification of PM2.5 in an arid Northwest US City by positive matrix factorization,
714   Atmospheric Research, 66, 291-305, 2003b.
715 Kim, J.-H., Park, J.-M., Lee, S.-B., Pudasainee, D., and Seo, Y.-C.: Anthropogenic mercury
716   emission inventory with emission factors and total emission in Korea, Atmos.
717   Environ., 44, 2714-2721, 2010.
718 Kim, K.-H., Brown, R. J., Kwon, E., Kim, I.-S., and Sohn, J.-R.: Atmospheric mercury at an
719   urban station in Korea across three decades, Atmos. Environ., 131, 124-132, 2016.

720 Kim, K.-H., and Kim, M.-Y.: The effects of anthropogenic sources on temporal distribution
721   characteristics of total gaseous mercury in Korea, Atmos. Environ., 34, 3337-3347,
722   2000.
723 Kim, K.-H., and Kim, M.-Y.: Some insights into short-term variability of total gaseous
724   mercury in urban air, Atmos. Environ., 35, 49-59, 2001.
725 Kim, S.-H., Han, Y.-J., Holsen, T. M., and Yi, S.-M.: Characteristics of atmospheric
726   speciated mercury concentrations (TGM, Hg (II) and Hg (p)) in Seoul, Korea, Atmos.
727   Environ., 43, 3267-3274, 2009.
728 Kuo, T.-H., Chang, C.-F., Urba, A., and Kvietkus, K.: Atmospheric gaseous mercury in
729   Northern Taiwan, Sci. Total Environ., 368, 10-18, 2006.
730 Lai, S.-O., Holsen, T. M., Hopke, P. K., and Liu, P.: Wet deposition of mercury at a New
731   York state rural site: concentrations, fluxes, and source areas, Atmos. Environ., 41,
732   4337-4348, 2007.
733 Laurier, F. J., Mason, R. P., Whalin, L., and Kato, S.: Reactive gaseous mercury formation in
734   the North Pacific Ocean's marine boundary layer: A potential role of halogen
735   chemistry, Journal of Geophysical Research: Atmospheres (1984–2012), 108, 2003.
736 Lee, D. S., Dollard, G. J., and Pepler, S.: Gas-phase mercury in the atmosphere of the United
737   Kingdom, Atmos. Environ., 32, 855-864, 1998.
738 Lee, S. J., Seo, Y.-C., Jurng, J., Hong, J.-H., Park, J.-W., Hyun, J. E., and Lee, T. G.:
739   Mercury emissions from selected stationary combustion sources in Korea, Sci. Total
740   Environ., 325, 155-161, 2004.
741 Li, Z., Xia, C., Wang, X., Xiang, Y., and Xie, Z.: Total gaseous mercury in Pearl River Delta
742   region, China during 2008 winter period, Atmos. Environ., 45, 834-838, 2011.
743 Lim, C.-J., Cheng, M.-D., and Schroeder, W. H.: Transport patterns and potential sources of
744   total gaseous mercury measured in Canadian high Arctic in 1995, Atmos. Environ.,
745   35, 1141-1154, 2001.
746 Lin, C.-J., and Pehkonen, S. O.: The chemistry of atmospheric mercury: a review, Atmos.
747   Environ., 33, 2067-2079, 1999.
748 Lin, C.-J., Pongprueksa, P., Lindberg, S. E., Pehkonen, S. O., Byun, D., and Jang, C.:
749   Scientific uncertainties in atmospheric mercury models I: Model science evaluation,
750   Atmos. Environ., 40, 2911-2928, 2006.
751 Lindberg, S., Bullock, R., Ebinghaus, R., Engstrom, D., Feng, X., Fitzgerald, W., Pirrone, N.,
752   Prestbo, E., and Seigneur, C.: A synthesis of progress and uncertainties in attributing
753   the sources of mercury in deposition, AMBIO: A Journal of the Human Environment,
754   36, 19-33, 2007.
755 Liu, N., Qiu, G., Landis, M. S., Feng, X., Fu, X., and Shang, L.: Atmospheric mercury
756   species measured in Guiyang, Guizhou province, southwest China, Atmospheric
757   Research, 100, 93-102, 2011.
758 Lu, J. Y., and Schroeder, W. H.: Annual time-series of total filterable atmospheric mercury
759   concentrations in the Arctic, Tellus B, 56, 213-222, 2004.
760 Lynam, M. M., and Keeler, G. J.: Source–receptor relationships for atmospheric mercury in
761   urban Detroit, Michigan, Atmos. Environ., 40, 3144-3155, 2006.
762 Mao, H., Talbot, R., Sigler, J., Sive, B., and Hegarty, J.: Seasonal and diurnal variations of
763   Hg over New England, Atmos. Chem. Phys., 8, 1403-1421, 2008.
764 Marumoto, K., Hayashi, M., and Takami, A.: Atmospheric mercury concentrations at two
765   sites in the Kyushu Islands, Japan, and evidence of long-range transport from East
766   Asia, Atmos. Environ., 117, 147-155, 2015.
767 Mason, R. P., and Sheu, G. R.: Role of the ocean in the global mercury cycle, Global
768   biogeochemical cycles, 16, 40-1-40-14, 2002.

769   Miller, C. L., Watson, D. B., Lester, B. P., Lowe, K. A., Pierce, E. M., and Liang, L.:
770   Characterization of soils from an industrial complex contaminated with elemental
771   mercury, Environ. Res., 125, 20-29, 2013.
772   Muntean, M., Janssens-Maenhout, G., Song, S., Selin, N. E., Olivier, J. G., Guizzardi, D.,
773   Maas, R., and Dentener, F.: Trend analysis from 1970 to 2008 and model evaluation
774   of EDGARv4 global gridded anthropogenic mercury emissions, Sci. Total Environ.,
775   494, 337-350, 2014.
776   Nakagawa, R.: Studies on the levels in atmospheric concentrations of mercury in Japan,
777   Chemosphere, 31, 2669-2676, 1995.
778   Nier: National Air Pollutants Emission 2011 (in Korean), 2011.
779   Obrist, D., Tas, E., Peleg, M., Matveev, V., Faïn, X., Asaf, D., and Luria, M.: Bromine-
780   induced oxidation of mercury in the mid-latitude atmosphere, Nature Geoscience, 4,
781   22-26, 2011.
782   Osawa, T., Ueno, T., and Fu, F.: Sequential variation of atmospheric mercury in Tokai-mura,
783   seaside area of eastern central Japan, Journal of Geophysical Research: Atmospheres
784   (1984–2012), 112, 2007.
785   Pacyna, E. G., Pacyna, J., Sundseth, K., Munthe, J., Kindbom, K., Wilson, S., Steenhuisen,
786   F., and Maxson, P.: Global emission of mercury to the atmosphere from
787   anthropogenic sources in 2005 and projections to 2020, Atmos. Environ., 44, 2487-
788   2499, 2010.
789   Pacyna, E. G., Pacyna, J. M., Steenhuisen, F., and Wilson, S.: Global anthropogenic mercury
790   emission inventory for 2000, Atmos. Environ., 40, 4048-4063, 2006.
791   Pacyna, J. M., Pacyna, E. G., Steenhuisen, F., and Wilson, S.: Mapping 1995 global
792   anthropogenic emissions of mercury, Atmos. Environ., 37, 109-117, 2003.
793   Pirrone, N., Aas, W., Cinnirella, S., Ebinghaus, R., Hedgecock, I. M., Pacyna, J., Sprovieri,
794   F., and Sunderland, E. M.: Toward the next generation of air quality monitoring:
795   Mercury, Atmos. Environ., 80, 599-611, 2013.
796   Pirrone, N., Cinnirella, S., Feng, X., Finkelman, R., Friedli, H., Leaner, J., Mason, R.,
797   Mukherjee, A., Stracher, G., and Streets, D.: Global mercury emissions to the
798   atmosphere from anthropogenic and natural sources, Atmospheric Chemistry and
799   Physics, 10, 5951-5964, 2010.
800   Poissant, L.: Potential sources of atmospheric total gaseous mercury in the St. Lawrence
801   River valley, Atmos. Environ., 33, 2537-2547, 1999.
802   Polissar, A. V., Hopke, P. K., and Harris, J. M.: Source regions for atmospheric aerosol
803   measured at Barrow, Alaska, Environ. Sci. Technol., 35, 4214-4226, 2001.
804   Sakata, M., and Marumoto, K.: Formation of atmospheric particulate mercury in the Tokyo
805   metropolitan area, Atmos. Environ., 36, 239-246, 2002.
806   Sakata, M., and Marumoto, K.: Wet and dry deposition fluxes of mercury in Japan, Atmos.
807   Environ., 39, 3139-3146, 2005.
808   Schmolke, S. R., Schroeder, W., Kock, H., Schneeberger, D., Munthe, J., and Ebinghaus, R.:
809   Simultaneous measurements of total gaseous mercury at four sites on a 800km
810   transect: spatial distribution and short-time variability of total gaseous mercury over
811   central Europe, Atmos. Environ., 33, 1725-1733, 1999.
812   Schroeder, W. H., and Munthe, J.: Atmospheric mercury—an overview, Atmos. Environ., 32,
813   809-822, 1998.
814   Seo, Y.-S., Han, Y.-J., Choi, H.-D., Holsen, T. M., and Yi, S.-M.: Characteristics of total
815   mercury (TM) wet deposition: scavenging of atmospheric mercury species, Atmos.
816   Environ., 49, 69-76, 2012.

817   Seo, Y.-S., Han, Y.-J., Holsen, T. M., Choi, E., Zoh, K.-D., and Yi, S.-M.: Source
818   identification of total mercury (TM) wet deposition using a Lagrangian particle
819   dispersion model (LPDM), Atmos. Environ., 104, 102-111, 2015.
820   Shon, Z.-H., Kim, K.-H., Kim, M.-Y., and Lee, M.: Modeling study of reactive gaseous
821   mercury in the urban air, Atmos. Environ., 39, 749-761, 2005.
822   Slemr, F., Brunke, E. G., Ebinghaus, R., Temme, C., Munthe, J., Wängberg, I., Schroeder,
823   W., Steffen, A., and Berg, T.: Worldwide trend of atmospheric mercury since 1977,
824   Geophys. Res. Lett., 30, 2003.
825   Song, X., Cheng, I., and Lu, J.: Annual atmospheric mercury species in downtown Toronto,
826   Canada, J. Environ. Monit., 11, 660-669, 2009.
827   Sprovieri, F., Pirrone, N., Ebinghaus, R., Kock, H., and Dommergue, A.: A review of
828   worldwide atmospheric mercury measurements, Atmos. Chem. Phys., 10, 8245-8265,
829   2010.
830   Stamenkovic, J., Lyman, S., and Gustin, M. S.: Seasonal and diel variation of atmospheric
831   mercury concentrations in the Reno (Nevada, USA) airshed, Atmos. Environ., 41,
832   6662-6672, 2007.
833   Stohl, A., Eckhardt, S., Forster, C., James, P., Spichtinger, N., and Seibert, P.: A replacement
834   for simple back trajectory calculations in the interpretation of atmospheric trace
835   substance measurements, Atmos. Environ., 36, 4635-4648, 2002.
836   Streets, D. G., Devane, M. K., Lu, Z., Bond, T. C., Sunderland, E. M., and Jacob, D. J.: All-
837   time releases of mercury to the atmosphere from human activities, Environ. Sci.
838   Technol., 45, 10485-10491, 2011.
839   Strode, S. A., Jaeglé, L., Selin, N. E., Jacob, D. J., Park, R. J., Yantosca, R. M., Mason, R. P.,
840   and Slemr, F.: Air-sea exchange in the global mercury cycle, Global Biogeochemical
841   Cycles, 21, 2007.
842   Temme, C., Blanchard, P., Steffen, A., Banic, C., Beauchamp, S., Poissant, L., Tordon, R.,
843   and Wiens, B.: Trend, seasonal and multivariate analysis study of total gaseous
844   mercury data from the Canadian atmospheric mercury measurement network
845   (CAMNet), Atmos. Environ., 41, 5423-5441, 2007.
846   Unep: *Global mercury assessment*. UNEP Chemicals, 2002.
847   Unep: The global atmospheric mercury assessment: Sources, emissions and transport,
848   http://www.unep.org/chemicalsandwaste/Portals/9/Mercury/Documents/Publications/
849   UNEP_GlobalAtmosphericMercuryAssessment_May2009.pdf, 2008.
850   Uria-Tellaetxe, I., and Carslaw, D. C.: Conditional bivariate probability function for source
851   identification, Environ. Model. Software, 59, 1-9, 2014.
852   Wan, Q., Feng, X., Lu, J., Zheng, W., Song, X., Han, S., and Xu, H.: Atmospheric mercury in
853   Changbai Mountain area, northeastern China I. The seasonal distribution pattern of
854   total gaseous mercury and its potential sources, Environ. Res., 109, 201-206, 2009.
855   Weigelt, A., Ebinghaus, R., Manning, A., Derwent, R., Simmonds, P., Spain, T., Jennings, S.,
856   and Slemr, F.: Analysis and interpretation of 18 years of mercury observations since
857   1996 at Mace Head, Ireland, Atmos. Environ., 100, 85-93, 2015.
858   Weiss-Penzias, P., Jaffe, D., Swartzendruber, P., Hafner, W., Chand, D., and Prestbo, E.:
859   Quantifying Asian and biomass burning sources of mercury using the Hg/CO ratio in
860   pollution plumes observed at the Mount Bachelor Observatory, Atmos. Environ., 41,
861   4366-4379, 2007.
862   Weiss-Penzias, P., Jaffe, D. A., Mcclintick, A., Prestbo, E. M., and Landis, M. S.: Gaseous
863   elemental mercury in the marine boundary layer: Evidence for rapid removal in
864   anthropogenic pollution, Environ. Sci. Technol., 37, 3755-3763, 2003.

865   Weiss-Penzias, P., Jaffe, D. A., Swartzendruber, P., Dennison, J. B., Chand, D., Hafner, W.,
866   and Prestbo, E.: Observations of Asian air pollution in the free troposphere at Mount
867   Bachelor Observatory during the spring of 2004, Journal of Geophysical Research:
868   Atmospheres (1984–2012), 111, 2006.
869   Wilson, S., Munthe, J., Sundseth, K., Maxson, P., Kindbom, K., Pacyna, J., and Steenhuisen,
870   F. Updating Historical Global Inventories of Anthropogenic Mercury Emissions to
871   Air. AMAP Technical Report No. 3 (2010). Arctic Monitoring and Assessment
872   Programme (AMAP). 2010.
873   Xie, Y., and Berkowitz, C. M.: The use of positive matrix factorization with conditional
874   probability functions in air quality studies: an application to hydrocarbon emissions in
875   Houston, Texas, Atmos. Environ., 40**,** 3070-3091, 2006.
876   Zeng, Y., and Hopke, P.: A study of the sources of acid precipitation in Ontario, Canada,
877   Atmospheric Environment (1967), 23**,** 1499-1509, 1989.
878   Zhang, H., and Lindberg, S. E.: Sunlight and iron (III)-induced photochemical production of
879   dissolved gaseous mercury in freshwater, Environ. Sci. Technol., 35**,** 928-935, 2001.
880   Zhang, L., Wang, S., Wang, L., Wu, Y., Duan, L., Wu, Q., Wang, F., Yang, M., Yang, H.,
881   Hao, J., and Liu, X.: Updated emission inventories for speciated atmospheric mercury
882   from anthropogenic sources in China, Environ. Sci. Technol., 49**,** 3185-94, 2015.
883   Zhao, W., Hopke, P. K., and Karl, T.: Source identification of volatile organic compounds in
884   Houston, Texas, Environ. Sci. Technol., 38**,** 1338-1347, 2004.
885   Zhou, L., Kim, E., Hopke, P. K., Stanier, C. O., and Pandis, S.: Advanced factor analysis on
886   Pittsburgh particle size-distribution data special issue of aerosol science and
887   technology on findings from the Fine Particulate Matter Supersites Program, Aerosol
888   Science and Technology, 38**,** 118-132, 2004.